

chromosomes of *Drosophila miranda* a model for sex chromosome evolution. *Genetica* **102**–103, 409–420 (1998).

10. Waters, P. D., Duffy, B., Frost, C. J., Delbridge, M. L. & Graves, J. A. The human Y chromosome derives largely from a single autosomal region added to the sex chromosomes 80–130 million years ago. *Cytogenet. Cell. Genet.* **92**, 74–79 (2001).
11. Das, M., Mutsuddi, D., Duttgupta, A. K. & Mukherjee, A. S. Segmental heterogeneity in replication and transcription of the X₂ chromosome of *Drosophila miranda* and conservativeness in the evolution of dosage compensation. *Chromosoma* **87**, 373–388 (1982).
12. Li, W. *Molecular Evolution* (Sinauer Associates, Sunderland, Massachusetts, 1997).
13. Yi, S. & Charlesworth, B. Contrasting patterns of molecular evolution of the genes on the new and old sex chromosomes of *Drosophila miranda*. *Mol. Biol. Evol.* **17**, 703–717 (2000).
14. Wang, R. L. & Hey, J. The speciation history of *Drosophila pseudoobscura* and close relatives: inferences from DNA sequence variation at the *period* locus. *Genetics* **144**, 1113–1126 (1996).
15. Kimura, M. *The Neutral Theory of Molecular Evolution* (Cambridge Univ. Press, Cambridge, 1983).
16. Wright, S. *Evolution and the Genetics of Populations* (Univ. of Chicago Press, Chicago, 1969).
17. Bachtrog, D. & Charlesworth, B. Reduced levels of microsatellite variability on the neo-Y chromosome of *Drosophila miranda*. *Curr. Biol.* **10**, 1025–1031 (2000).
18. Filatov, D. A., Moneger, F., Negritiu, I. & Charlesworth, D. Low variability in a Y-linked plant gene and its implications for Y-chromosome evolution. *Nature* **404**, 388–390 (2000).
19. Yang, Z. PAML: a program package for phylogenetic analysis by maximum likelihood. *Comput. Appl. Biosci.* **13**, 555–556 (1997).
20. McDonald, J. H. & Kreitman, M. Adaptive protein evolution at the *Adh* locus in *Drosophila*. *Nature* **351**, 652–654 (1991).
21. Barton, N. H. Genetic hitchhiking. *Phil. Trans. R. Soc. Lond. B* **355**, 1553–1562 (2000).
22. Hudson, R. R., Kreitman, M. & Aguade, M. A test of neutral molecular evolution based on nucleotide data. *Genetics* **116**, 153–159 (1987).
23. Lynch, M. & Blanchard, J. L. Deleterious mutation accumulation in organelle genomes. *Genetica* **102**–103, 29–39 (1998).
24. Fridolfsson, A. K. & Ellegren, H. Molecular evolution of the avian *CHD1* genes on the Z and W sex chromosomes. *Genetics* **155**, 1903–1912 (2000).
25. Maynard Smith, J. *The Evolution of Sex* (Cambridge Univ. Press, Cambridge, 1978).
26. Barton, N. H. & Charlesworth, B. Why sex and recombination? *Science* **281**, 1986–1990 (1998).
27. Bell, G. *The Masterpiece of Nature* (Univ. of California, Berkeley, 1982).
28. Tajima, F. Statistical analysis of DNA polymorphism. *Jpn J. Genet.* **68**, 567–595 (1993).
29. Hudson, R. R. in *Oxford Surveys in Evolutionary Biology* Vol. 7 (eds Futuyma, D. & Antonovics, J.) 1–44 (Oxford Univ. Press, Oxford, 1990).
30. Weiss, G. & von Haeseler, A. Inference of population history using a likelihood approach. *Genetics* **149**, 1539–1546 (1998).

Acknowledgements

We thank P. Andolfatto, N. Barton, D. Charlesworth, I. Gordo, P. Keightley and S. Wright for helpful comments on the manuscript. D.B. is supported by a Marie Curie fellowship and B.C. by the Royal Society.

Competing interests statement

The authors declare that they have no competing financial interests.

Correspondence and requests for materials should be addressed to D.B. (e-mail: doris.bachtrog@ed.ac.uk).

Dissecting the architecture of a quantitative trait locus in yeast

Lars M. Steinmetz*†, Himanshu Sinha‡, Dan R. Richards*, Jamie I. Spiegelman†, Peter J. Oefner†§, John H. McCusker‡ & Ronald W. Davis*†§

Departments of * Genetics and § Biochemistry, Stanford University School of Medicine, Stanford, California 94305, USA

† Stanford Genome Technology Center, 855 California Avenue, Palo Alto, California 94304, USA

‡ Department of Microbiology, Duke University Medical Center, Durham, North Carolina 27710, USA

Most phenotypic diversity in natural populations is characterized by differences in degree rather than in kind. Identification of the actual genes underlying these quantitative traits has proved difficult^{1–5}. As a result, little is known about their genetic architecture. The failures are thought to be due to the different contributions of many underlying genes to the phenotype and

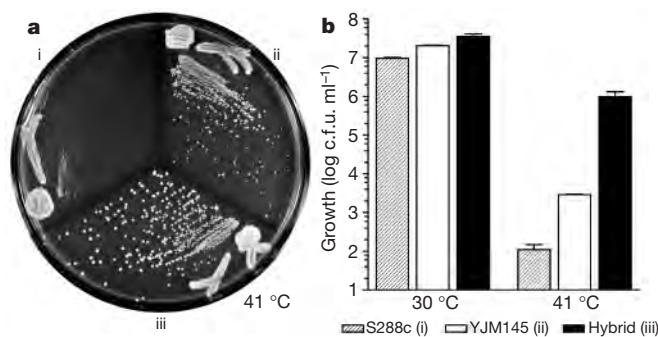


Figure 1 Analysis of the high-temperature-growth phenotype (Htg). **a**, Qualitative differences measured by colony size; **b**, quantitative differences in growth measured by competition assay after 48 h at 30 and 41 °C: (i) S1029, an Htg⁻ S288c strain, (ii) YAG040, an Htg⁺ YJM145 strain, and (iii) XHS123, a YJM145/S288c hybrid. Bars indicate s.e.m. (*n* = 6).

the ability of different combinations of genes and environmental factors to produce similar phenotypes^{6,7}. This study combined genome-wide mapping and a new genetic technique named reciprocal-hemizyosity analysis to achieve the complete dissection of a quantitative trait locus (QTL) in *Saccharomyces cerevisiae*. A QTL architecture was uncovered that was more complex than expected. Functional linkages both *in cis* and *in trans* were found between three tightly linked quantitative trait genes that are neither necessary nor sufficient in isolation. This arrangement of alleles explains heterosis (hybrid vigour), the increased fitness of the heterozygote compared with homozygotes. It also demonstrates a deficiency in current approaches to QTL dissection with implications extending to traits in other organisms, including human genetic diseases.

We chose the high-temperature-growth phenotype (Htg), common to clinically derived yeast isolates^{8–10} as a quantitative trait, because this ability is correlated with virulence in studies of infected mice¹¹. We selected two *S. cerevisiae* genetic backgrounds for study. YJM145 is a homozygous diploid strain⁸ that was generated from a heterozygous clinical isolate obtained from the lung of an AIDS patient¹². In contrast, S288c, a commonly used haploid laboratory genetic background for which the whole genome sequence is known, was derived from a strain isolated from a rotten fig¹³.

The respective Htg phenotypes of YJM145, S288c and a diploid hybrid of the two strains (designated YJM145/S288c) were determined by using a colony-size assay (Fig. 1a) and a quantitative competition assay (Fig. 1b). Both assays showed that a diploidized S288c strain grows poorly at high temperature (Htg⁻) relative to YJM145 (Htg⁺). In addition, both assays demonstrated that the hybrid displays heterosis. These data suggested that Htg is co-dominant and that both the clinical and the laboratory genetic backgrounds contain alleles that contribute to the Htg⁺ phenotype of the hybrid.

To analyse the heritability of the Htg phenotype, we sporulated a hybrid that was generated by crossing YJM789, a haploid strain isogenic with YJM145, with S96, a haploid strain isogenic with S288c. Each haploid progeny (segregant) was tested for growth at 41 °C with the use of the colony size assay. The segregants exhibited a wide range of Htg phenotypes, but, interestingly, none of the segregants were as Htg⁺ as the hybrid. Only 104 of 960 segregants (240 tetrads) were at least as Htg⁺ as YJM789 and were selected for further analysis. At this Htg⁺ threshold, defining Htg⁺, the 1:9 inheritance ratio predicted at least 3.2 underlying genetic loci (1/9 = 1/2^{3.2}). However, because Htg is quantitative and could be conditioned by combinations of alleles that are each neither

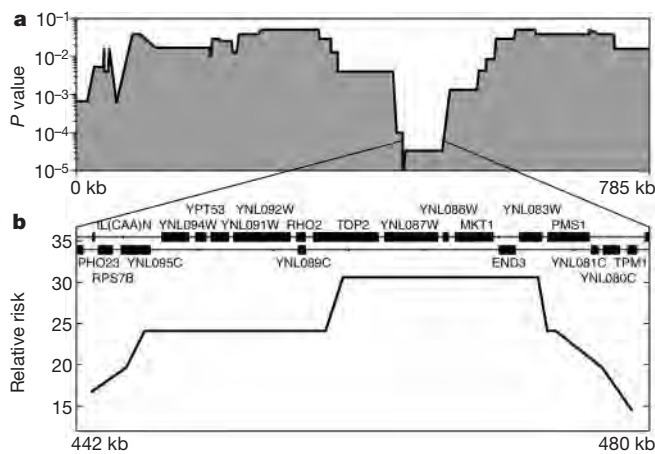


Figure 2 Detection by genome-wide mapping and detailed analysis by fine-structure mapping of the chromosome XIV Htg QTL. **a**, Calculated probability assuming random segregation (y -axis) for 3,444 markers in a whole-genome allelic variation scan of 19 Htg⁺ segregants, shown here for chromosome XIV. A region with low probability was identified between bp 434,194 and 485,856. **b**, Relative-risk plot representing the fine-structure map of the low-probability region. From 104 Htg⁺ segregants, the recombination breakpoints defining an interval with high relative risk were placed to within 32 kb (bp 445,003–477,059 of chromosome XIV).

necessary nor sufficient, the prediction of an exact number of loci is impossible.

A QTL mapping strategy was devised to detect the major Htg⁺ contributors from either genetic background. To identify DNA markers, total genomic DNAs from YJM789 and S96 were hybridized separately to Affymetrix high-density oligonucleotide arrays containing several probes to every open reading frame (ORF) of the yeast genome^{14,15}. A total of 3,444 biallelic markers were identified from probes with decreased signal strength in YJM789 relative to S96–DNA hybridizations, yielding an average marker spacing over the entire genome of 3,504 base pairs (bp), corresponding to an average genetic distance of 1.2 centimorgans (cM).

To maximize the ability to detect QTLs by genotyping the extreme phenotype progeny¹⁶, 19 of the selected 104 Htg⁺ segregants were analysed in genome-wide scans. Genomic DNA from each Htg⁺ segregant was hybridized to a high-density oligonucleotide array. The most probable parental origin for each DNA interval was determined from the hybridization signal. Meiotic recombination breakpoints were identified and compared for all Htg⁺ segregants, to find genomic intervals inherited from the same parent in a significant number of segregants. Two intervals with a low probability

(P) of random segregation were identified: one on chromosome XIV (51.6 kilobases (kb) in size, $P \approx 1/30,000$) and one on chromosome XVI (8.1 kb, $P \approx 1/20,000$).

To confirm the heritability of both intervals and to define precisely the QTL regions, the inheritance of multiple markers in all 104 Htg⁺ segregants was examined. With the use of denaturing high-performance liquid chromatography (DHPLC), 21 markers in the chromosome XVI interval and 28 markers in the chromosome XIV interval were identified and genotyped. The chromosome XVI QTL had a low but significant level of Htg⁺ association: of 104 Htg⁺ segregants, 66.7% inherited YJM145-derived alleles in an interval between 298,521 and 301,584 bp. This percentage translated to a relative risk of 2.1, namely the probability of being Htg⁺ is increased 2.1-fold if a strain carries the YJM145-derived rather than the S288c-derived alleles for this interval. Given its low relative risk, the chromosome XVI interval was not examined further.

A far greater Htg⁺ association was identified for the chromosome XIV QTL: 96.2% of the Htg⁺ segregants inherited the YJM145-derived alleles, yielding a relative risk of 30.6. A peak of 14.9 kb was mapped inside a larger interval of 32 kb (Fig. 2). Interestingly, the interval size was larger than the expected ~6 kb or 2 cM, based on the almost 100% Htg⁺ association (200 cM/104 segregants)¹⁷.

Two lines of evidence further strengthened the association of the chromosome XIV interval with Htg⁺. First, random segregants from the same cross displayed random segregation of the QTL¹⁴. Second, DHPLC analysis of 64 Htg⁺ segregants from a similar cross between an Htg⁻ S288c background strain and an unrelated Htg⁺ clinical strain, isogenic with YJM421⁸, showed 87.5% Htg⁺ association (position 468,445) (L.M.S. and J.H.M., unpublished data). The high but incomplete association of the chromosome XIV interval in both crosses confirmed that it is a major-effect QTL, yet neither necessary nor sufficient to condition Htg⁺ in the segregants.

To identify the phenotypically relevant alleles, we performed a detailed sequence analysis of the chromosome XIV interval. In addition to identifying the differences between YJM145 and S288c-derived alleles, the purpose of this comparative sequence analysis was to test the assumption of marker–trait association, namely that phenotypically relevant Htg⁺ sequence variants would be more prevalent in Htg⁺ strains than in Htg⁻ strains. The entire 32 kb interval (445,003–477,059) was therefore sequenced from six Htg⁺ and seven Htg⁻ strains. All Htg⁺ strains are segregants of clinical isolates (Fig. 3, rows a–f), whereas the Htg⁻ strains consist of common laboratory strains (Fig. 3, rows i and k–m), and segregants of wine (row g), grape (row h) and distillery (row j) strains. In total, 374 sequence variants were identified that define a phylogenetic relationship between the strains (see Supplementary Information).

Between YJM789 and S96, 83 sequence variants (1/385 base pairs) were detected, of which 24 were non-synonymous, including three insertion–deletions in YNL089C (457,139), PMS1 (473,368) and

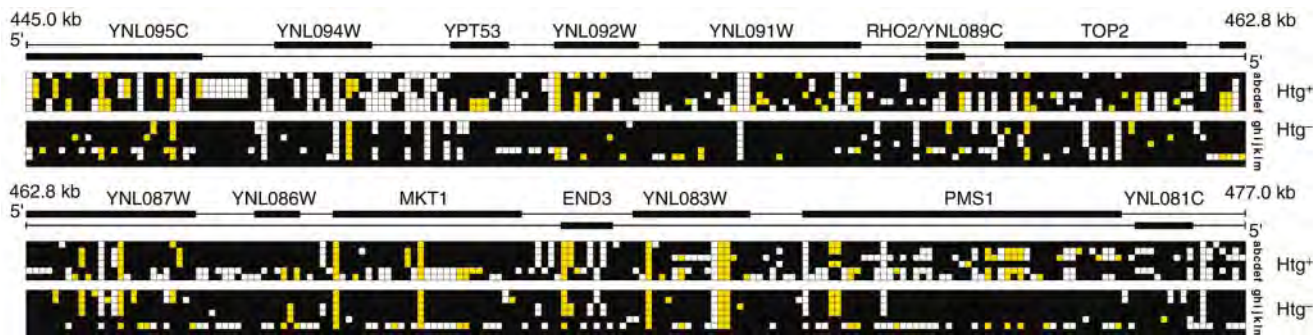


Figure 3 Sequence variations in chromosome XIV QTL between YJM789 (YJM145 genetic background), S96 (S288c background) and five other Htg⁺ and six other Htg⁻ yeast strains. Each column represents a sequence variant relative to S288c; non-

synonymous variants are coloured in yellow. Rows a–f show Htg⁺ strains: YJM789 (a), YJM326 (b), YJM320 (c), YJM280 (d), YJM421 (e), YJM339 (f). Rows g–m show Htg⁻ strains: YJM270 (g), YJM269 (h), YJM627 (i), YJM1129 (j), W303 (k), SK1 (l), S96 (m).

YNL083W (472,573) that encoded two truncated and one extended protein product in YJM789, respectively. Ten non-synonymous variants with identical sequences for all Htg⁺ strains were found in *YNL095C*, *YNL092W*, *YNL087W*, *YNL083W* and *MKT1*. However, many of the Htg⁻ strains shared the same sequences, eliminating the significance of the association. Low and incomplete levels of association were also observed for variants in *YNL095W*, *YNL091W* and *PMS1*.

In addition to the limited marker-trait association, none of the genes in the chromosome XIV QTL showed mRNA transcript level differences of threefold or greater in a genome-wide expression analysis of YJM789 and S96 at 30 and 37 °C (see Supplementary Information). Consequently, we developed a new functional assay named reciprocal-hemizyosity analysis to identify the phenotypically relevant allele(s).

Reciprocal-hemizyosity analysis is a tool for analysing each allele

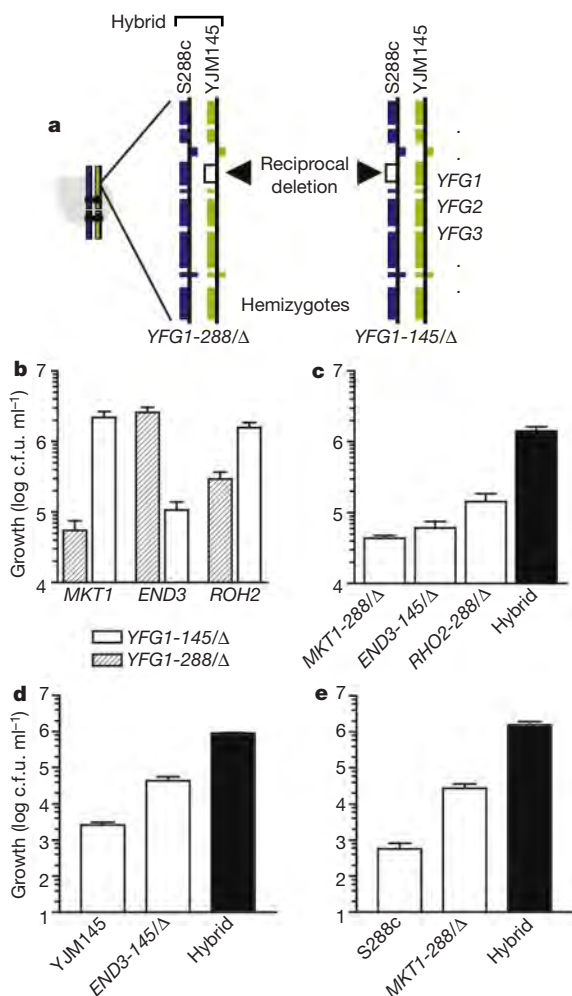


Figure 4 Reciprocal-hemizyosity analysis. **a**, Comparison between reciprocal *YFG1* hemizygotes (a generic gene name). Each block represents a gene. Each hemizygote carries only a single allele of *YFG1* but has an otherwise hybrid diploid genome. Two different dominant drug markers (open boxes) distinguish between competing reciprocal strains. **b**, Reciprocal-hemizyosity analysis of *MKT1*, *END3* and *RHO2* at 41 °C. For each gene pair, 12 measurements ($n = 12$) were taken to calculate the growth mean (c.f.u. ml⁻¹) and s.e.m. **c**, Htg contributions of *MKT1-145*, *END3-288* and *RHO2-145* alleles ($n = 12$). **d**, Role of S288c-derived alleles in heterosis. Competitions between YAG040 (Htg⁺ YJM145 background) and the hybrids, XHS122 (*END3-145/Δ*) and XHS123 (YJM145/S288c) ($n = 6$). **e**, Role of YJM145-derived alleles in heterosis. Competitions between S1029 (Htg⁻ S288c background) and the hybrids, XHS119 (*MKT1-288/Δ*) and XHS123 ($n = 6$).

in a hybrid genetic background. We applied reciprocal-hemizyosity analysis to all 15 genes in the chromosome XIV QTL. Isogenic pairs of strains were constructed in the hybrid background (YJM145/S288c) that differed genetically only in the alleles of one gene. In each strain one allele of one gene was deleted, producing a hemizygous diploid carrying either the S288c-derived or the YJM145-derived allele only (Fig. 4a). With reciprocal-hemizyosity analysis, we tested whether an allele from one genetic background was advantageous over that from the other by measuring competitive growth between reciprocal strains.

Because the phenotype is measured in hemizygotes and the identification of QTL alleles relies on a comparison between reciprocal strains, the approach also works for essential genes and is insensitive to potentially confounding gene dosage effects. As measurements are made in the hybrid strain background, segregating alleles from both S288c and YJM145 genetic backgrounds can be detected in one assay. In addition, segregating alleles inactive in each single genetic background but functional in combination with alleles from the other strain background can be discovered. Although our analysis used only single gene deletions, deletion combinations can be used to capture potential synergistic effects contributed by pairs of genes.

All allelic pairs, including the essential gene *TOP2*, were tested at 30, 40 and 41 °C. Strains containing only S288c-derived or YJM145-derived alleles of *YNL095W*, *YNL094W*, *YPT53*, *YNL092W*, *YNL091W*, *TOP2*, *YNL087W*, *YNL086W* and *YNL081C* grew equivalently at all temperatures. Htg differences were also not detected between alleles of *YNL083W* and *PMS1* containing the insertion-deletions. However, the spot dilution experiments showed growth differences for *MKT1*, *END3* and *RHO2*.

RHO2 overlaps with *YNL089C* and these two ORFs cannot be distinguished by deletion analysis. However, it seems that *YNL089C* is not a true ORF: its transcript was not detected in mRNA hybridizations to high-density arrays; three stop codons disrupt the homologous *Candida albicans* sequence; and a recent computational re-annotation of the *S. cerevisiae* genome defined *YNL089C* as a spurious ORF¹⁸. We therefore eliminated *YNL089C* from further consideration.

For *MKT1* and *RHO2*, the YJM145-derived alleles (*MKT1-145* and *RHO2-145*) were found to confer an Htg⁺ advantage. As determined by the more quantitative plating assay, no significant phenotypic differences were observed between reciprocal hemizygotes after 48 hours at 30 °C. However, at 40 °C the differences were significant. At 41 °C, a 40-fold growth difference was observed between isogenic *MKT1-145/Δ* and *MKT1-288/Δ* hemizygotes and a 5.5-fold difference between the respective *RHO2* hemizygotes ($P < 0.001$) (Fig. 4b).

Surprisingly, for *END3* the S288c-derived allele (*END3-288*) and not the YJM145-derived allele accounted for a 23.6-fold difference

Amino-acid position:	MKT1								END3			RHO2		Htg	
	30	106	337	432	453	600	610	657	806	245	258	268	91	150	
YJM789	G	S	F	A	R	F	S	V	A	D	N	N	C	I	+
YJM326	G	S	F	G	R	F	S	V	A	D	N	N	F	I	+
YJM320	G	S	F	G	R	F	S	V	A	D	N	N	F	I	+
YJM280	G	S	F	G	R	F	S	V	A	D	N	N	F	I	+
YJM421	G	S	F	A	R	L	R	I	A	E	S	N	F	I	+
YJM339	G	T	F	A	R	L	R	V	A	D	S	N	F	I	+
YJM270	G	S	F	A	R	F	S	V	A	D	S	N	F	V	-
YJM269	G	S	F	A	R	F	S	V	V	D	S	N	F	V	-
YJM627	G	S	F	A	R	F	S	V	A	D	N	N	F	I	-
YJM1129	G	S	F	A	R	F	S	V	A	D	N	N	F	I	-
W303	G	S	F	A	R	F	S	V	A	D	S	D	C	I	-
SK1	G	S	S	A	R	L	R	V	A	D	S	N	F	I	-
S96	D	S	F	A	K	F	S	V	A	D	S	D	F	I	-

Figure 5 Comparisons of the protein sequence polymorphisms for identified Htg⁺ genes among Htg⁺ and Htg⁻ strains. Amino acid residues are shaded in grey when identical to the Htg⁺ allele sequence. Residues are marked with an asterisk if they are different between the YJM145 and S288c genetic backgrounds.

in growth between isogenic *END3-288/Δ* and *END3-145/Δ* hemizygotes ($P < 0.001$). Although finding an Htg^+ allele from the laboratory-derived strain was not predicted by genetic mapping, the positive contribution of *END3-288* to Htg immediately suggested a possible explanation for both the failure to obtain segregants as Htg^+ as the hybrid and for the heterosis seen in crosses between S288c and YJM145 background strains (Fig. 1).

By measuring the relative contribution of each Htg^+ allele in a series of competitions between a hybrid (YJM145/S288c) and, in each case, two hemizygous hybrids that lacked one different Htg^+ allele, the contribution of alleles was found to be greatest for *MKT1-145* and lowest for *RHO2-145* (Fig. 4c). As a control, we confirmed that gene dosage does not affect phenotype: deletion of the Htg^- alleles (*MKT1-288*, *END3-145* and *RHO2-288*) in hybrid strains and hemizygous deletions of Htg^+ alleles in homozygous YJM145 diploid strains had no detectable phenotypic effect (see Supplementary Information).

The identified Htg^+ alleles are not sufficient to explain the contribution of each genetic background to heterosis. *END3-288* is a significant contributor to the Htg^+ phenotype of the hybrid, as its removal eliminated 48% of the growth advantage of the hybrid over YJM145 (Fig. 4d). However, the remaining Htg^+ phenotype of the *END3-145/Δ* hemizygote suggests the presence of at least one other Htg^+ S288c-derived allele. Removal of *MKT1-145*, the more significant of the two identified YJM145 Htg^+ contributors, eliminated 51% of the growth difference between the hybrid and the laboratory strain (Fig. 4e). Consistent with the already identified *RHO2-145* allele, the remaining Htg^+ phenotype suggests the presence of additional YJM145-derived QTLs.

The fact that neither of the identified alleles is necessary or sufficient is also consistent with a comparison of the protein sequences between Htg^+ and Htg^- strains. There are missense variants in Htg^+ alleles that are common in both populations (Fig. 5) and there are Htg^- strains with Htg^+ protein sequence variants and some with proven Htg^+ functionality (such as *END3-288* in S96) and vice versa. The lack of a single haplotype for all Htg^+ strains indicates that different allele combinations might contribute to Htg in different strains. These results are striking in view of the fact that the lack of differences in mRNA levels in these genes, and the lack of gene dosage effects on Htg , indicate that the Htg phenotype might be caused not by differences in transcription but by changes in protein function. Whereas the function of Mkt1p is unknown, apart from its role in the maintenance of the M2 double-stranded RNA virus above 30 °C (ref. 19), End3p and Rho2p are involved in the cytoskeleton.

Finding three Htg^+ alleles in a single mapped QTL provided immediate explanations for several observations. The two YJM145-derived contributors explain the detection of the QTL, their linkage *in cis* explains the larger than expected map interval, and the identification of the additional S288c-derived contributor *in trans* explains heterosis. The fact that neither single allele is necessary or sufficient for Htg^+ explains the lack of marker–trait association.

These findings indicate that existing approaches to quantitative traits demand re-evaluation. Combinations of both common and rare variants are likely to underlie quantitative traits and the number of genes could be far greater than expected. If closely linked loci are common, current single-gene-per-locus approaches might have intrinsic deficiencies. Although narrowing an interval in the hope of achieving a map interval that approaches a single point might serve to locate the major contributor, the effects of neighbouring genetic factors could be missed. In addition, many QTLs located throughout the genome might not be detected because of their small effect or their location *in trans* with another QTL allele. A more comprehensive approach to QTL dissection therefore needs to include one in which multiple genes can be tested individually and in combination. The reciprocal-hemizygosity analysis has the

potential of being applied genome-wide in model organisms. By using drug resistance markers in combination with molecular barcode tags²⁰, it might be possible to expand our analysis to measuring the phenotypic contribution of all allelic differences between two yeast genomes in a single step. □

Methods

Yeast growth media and strain construction

YPD medium, containing G418 (200 μg ml⁻¹), hygromycin B (300 μg ml⁻¹) or nourseothricin (100 μg ml⁻¹), was used to select strains with *kanMX4*, *hphMX4* and *natMX4* dominant drug-resistance markers^{21,22}. Haploid S288c background strains were diploidized²³. All deletion mutations were constructed in diploids by replacing specific ORFs with dominant drug-resistance cassettes^{21,22}; homologous integration was verified by colony polymerase chain reaction (PCR)²⁴ at both ends of integrated cassettes. Reciprocal hemizygous diploid strains were made with different, phenotypically neutral²¹ dominant drug markers to distinguish between competing strains. As a test of reproducibility, ORFs were replaced with both *hphMX4* and *natMX4* cassettes.

To construct isogenic hemizygous diploids containing only S288c-derived or only YJM145-derived alleles of specific genes, diploid S288c and YJM145 background strains carrying *lys2* or *lys5* mutations, with and without a hemizygous deletion of a gene (see Supplementary Information), were sporulated²⁵. To generate reciprocal pairs, spore suspensions from homozygous S288c and hemizygous YJM145 background diploids were mixed and vice versa. Mixtures were incubated overnight at 30 °C on YPD medium to allow mating between haploid spores, and then replica-plated onto SD medium to select for *Lys+* diploids. *Lys+* diploids were streaked onto the appropriate drug plate to isolate YJM145/S288c diploids hemizygous at a specific gene. See Supplementary Information for a table of strains.

Phenotypic determination of high-temperature growth

Colony size⁸ measured in duplicate was primarily used to determine the Htg phenotype of segregants, because Htg was more reproducible on plates than in liquid culture. After growth overnight at 30 °C, strains were streaked onto fresh YPD plates to obtain single colonies. After incubation for 48 h at 41 °C, colony size was compared with that of a YJM789 control; measurements above this threshold were defined as Htg^+ .

In reciprocal-hemizygosity analysis, one hemizygote carrying only an S288c-derived allele and another carrying only a YJM145-derived allele of a gene were competed, each marked with a different dominant drug marker. Each hemizygote in a pair was grown separately overnight at 30 °C in liquid YPD; cells from both cultures were mixed and diluted to ~10⁷ cells ml⁻¹. A 1 ml sample of this cell mixture (plus 4 ml sterile water to improve cell dispersal) was placed onto nitrocellulose filter papers 90 mm in diameter and with a pore size of 0.22 μm; the vacuum-dried filters were put on YPD plates and incubated at 30, 40 and 41 °C for 48 h. After incubation, the cells were recovered in 5 ml sterile water and tenfold serial dilutions were spotted onto drug plates. The dilution factor at which no growth was observed was compared for each hemizygote in a pair. For all genes in the Htg region, this serial-dilution-spotting assay was performed twice with each of two pairs of hemizygous diploids (dominant drug markers swapped).

In addition to the parental strains in Fig. 1, the *RHO2/Δ*, *MKT1/Δ* and *END3/Δ* hemizygotes, which showed allele-specific Htg differences in the dilution-spotting assay, were compared by spreading the dilutions of the suspensions to single colonies onto different drug plates that were incubated at 30 °C for 48 h. After incubation, the numbers of colonies growing on each drug plate were counted to calculate colony-forming units (c.f.u.) ml⁻¹. These competitions were performed twice with each of four pairs of hemizygous diploids to calculate growth means and their standard errors.

Genetic typing and expression analysis

For genome scans, total genomic DNA was fragmented, labelled and hybridized to Affymetrix Ye6100 yeast arrays. Biallelic markers were determined by the decreased hybridization efficiency of YJM789 relative to S96 (ref. 14). Additional markers for fine-structure mapping were identified and genotyped by DHPLC²⁶. Dideoxy sequencing was performed on ~600-bp PCR products tiled over the 32-kb interval with ~50 bp overlaps with the use of big dye terminators. Gene expression analysis was performed on Affymetrix Ye6100 yeast arrays from cultures grown in liquid YPD medium to 2 × 10⁷ cells ml⁻¹; mRNA was processed as described²⁷.

Statistical analysis

The Htg^+ segregant set included pairs from the same tetrad and segregants from unrelated meioses. To increase mapping power, segregant pairs were favoured for the genome-wide scan. The probability of observing a given marker segregation by chance was calculated as a product of multinomial and binomial probabilities that took into account the presence of Htg^+ segregant pairs:

$$p = \binom{n!}{a!b!c!} (1/6)^a (2/3)^b (1/6)^c C(m, k) 2^{-m}$$

given the number of segregant pairs n , of which b have different genotype, a the same YJM789 genotype, and c the same S96 genotype, and given the number of unrelated segregants m , of which k have the YJM789 genotype. Relative risk r was estimated, assuming that the risk for Htg^+ is independent for segregants of a pair, by maximizing the

likelihood function:

$$\left(\frac{r^2}{r^2 + 4r + 1}\right)^a \left(\frac{4r}{r^2 + 4r + 1}\right)^b \left(\frac{1}{r^2 + 4r + 1}\right)^c \left(\frac{r}{r+1}\right)^k \left(\frac{1}{r+1}\right)^{m-k}$$

where r represents the ratio of Htg⁺ probability given YJM145 genotype over that given S288c; other variables as above. For Htg competitions, t -tests were performed to determine the significance of differences in means. Percentage growth deficiency was calculated as $100(\log C - \log B)/(\log C - \log A)$, where A corresponds to c.f.u. ml⁻¹ of the control, B to that of the hemizygote, and C to that of the hybrid.

Received 9 August 2001; accepted 25 January 2002.

- Lander, E. S. & Schork, N. J. Genetic dissection of complex traits. *Science* **265**, 2037–2048 (1994).
- Risch, N. J. Searching for genetic determinants in the new millennium. *Nature* **405**, 847–856 (2000).
- Darvasi, A. Experimental strategies for the genetic dissection of complex traits in animal models. *Nature Genet.* **18**, 19–24 (1998).
- Mackay, T. F. Quantitative trait loci in *Drosophila*. *Nature Rev. Genet.* **2**, 11–20 (2001).
- Mauricio, R. Mapping quantitative trait loci in plants: uses and caveats for evolutionary biology. *Nature Rev. Genet.* **2**, 370–381 (2001).
- Flint, J. & Mott, R. Finding the molecular basis of quantitative traits: successes and pitfalls. *Nature Rev. Genet.* **2**, 437–445 (2001).
- Schafer, A. J. & Hawkins, J. R. DNA variation and the future of human genetics. *Nature Biotechnol.* **16**, 33–39 (1998).
- McCusker, J. H., Clemons, K. V., Stevens, D. A. & Davis, R. W. Genetic characterization of pathogenic *Saccharomyces cerevisiae* isolates. *Genetics* **136**, 1261–1269 (1994).
- Clemons, K. V., McCusker, J. H., Davis, R. W. & Stevens, D. A. Comparative pathogenesis of clinical and nonclinical isolates of *Saccharomyces cerevisiae*. *J. Infect. Dis.* **169**, 859–867 (1994).
- Murphy, A. & Kavanagh, K. Emergence of *Saccharomyces cerevisiae* as a human pathogen: Implications for biotechnology. *Enzyme Microb. Technol.* **25**, 551–557 (1999).
- McCusker, J. H., Clemons, K. V., Stevens, D. A. & Davis, R. W. *Saccharomyces cerevisiae* virulence phenotype as determined with CD-1 mice is associated with the ability to grow at 42°C and form pseudohyphae. *Infect. Immun.* **62**, 5447–5455 (1994).
- Tawfik, O. W., Papsian, C. J., Dixon, A. Y. & Potter, L. M. *Saccharomyces cerevisiae* pneumonia in a patient with acquired immune deficiency syndrome. *J. Clin. Microbiol.* **27**, 1689–1691 (1989).
- Mortimer, R. K. & Johnston, J. R. Genealogy of principal strains of the yeast genetic stock center. *Genetics* **113**, 35–43 (1986).
- Winzler, E. A. *et al.* Direct allelic variation scanning of the yeast genome. *Science* **281**, 1194–1197 (1998).
- Steinmetz, L. M. & Davis, R. W. High-density arrays and insights into genome function. *Biotechnol. Gen. Eng. Rev.* **17**, 109–146 (2000).
- Lander, E. S. & Botstein, D. Mapping mendelian factors underlying quantitative traits using RFLP linkage maps. *Genetics* **121**, 185–199 (1989).
- Boehnke, M. Limits of resolution of genetic linkage studies: implications for the positional cloning of human disease genes. *Am. J. Hum. Genet.* **55**, 379–390 (1994).
- Wood, V., Rutherford, K. M., Ivens, A., Rajandream, M. A. & Barrell, B. A re-annotation of the *Saccharomyces cerevisiae* genome. *Comp. Funct. Genom.* **2**, 143–154 (2001).
- Wickner, R. B. MKT1, a nonessential *Saccharomyces cerevisiae* gene with a temperature-dependent effect on replication of M2 double-stranded RNA. *J. Bacteriol.* **169**, 4941–4945 (1987).
- Shoemaker, D. D., Lashkari, D. A., Morris, D., Mittmann, M. & Davis, R. W. Quantitative phenotypic analysis of yeast deletion mutants using a highly parallel molecular bar-coding strategy. *Nature Genet.* **14**, 450–456 (1996).
- Goldstein, A. L. & McCusker, J. H. Three new dominant drug resistance cassettes for gene disruption in *Saccharomyces cerevisiae*. *Yeast* **15**, 1541–1553 (1999).
- Wach, A., Brachat, A., Pohlmann, R. & Philippsen, P. New heterologous modules for classical or PCR-based gene disruptions in *Saccharomyces cerevisiae*. *Yeast* **10**, 1793–1808 (1994).
- Herskowitz, I. & Jensen, R. E. in *Methods in Enzymology* (eds Guthrie, C. & Fink, G. R.) 132–246 (Academic, San Diego, 1991).
- Niedenthal, R. K., Riles, L., Johnston, M. & Hegemann, J. H. Green fluorescent protein as a marker for gene expression and subcellular localization in budding yeast. *Yeast* **12**, 773–786 (1996).
- Codon, A. C., Gasent-Ramirez, J. M. & Benitez, T. Factors which affect the frequency of sporulation and tetrad formation in *Saccharomyces cerevisiae* baker's yeasts. *Appl. Environ. Microbiol.* **61**, 630–638 (1995).
- Spiegelman, J. I. *et al.* Cloning of the *Arabidopsis* RSF1 gene by using a mapping strategy based on high-density DNA arrays and denaturing high-performance liquid chromatography. *Plant Cell* **12**, 2485–2498 (2000).
- Primig, M. *et al.* The core meiotic transcriptome in budding yeasts. *Nature Genet.* **26**, 415–423 (2000).

Supplementary Information accompanies the paper on Nature's website (<http://www.nature.com>).

Acknowledgements

We thank N. Risch, E. Mignot, K. White, R. Hyman, J. Haber, C. Scharfe, T. Jones and M. Mindrinos for helpful discussion, and M. Trebo for help in preparing the website. This work was supported by the NIH (P.J.O., J.H.M. and R.W.D.) and by a Howard Hughes Medical Institute predoctoral fellowship awarded to L.M.S. Strain phenotyping and reciprocal-hemizygosity analysis were performed at Duke University; mapping, expression and sequence analysis were done at Stanford University.

Correspondence and requests for materials should be addressed to J.H.M. (e-mail: mccus001@mc.duke.edu) or L.M.S. (e-mail: larsms@stanford.edu). Sequences have been deposited in GenBank under the following accession numbers: S96 (AF458969), YJM280 (AF458970), YJM320 (AF458971), YJM326 (AF458972), YJM339 (AF458973), YJM421 (AF458974), YJM789 (AF458975), SK1 (AF458976), W303 (AF458977), YJM1129 (AF458978), YJM269 (AF458979), YJM270 (AF458980), YJM627 (AF458981).

Inhibition of climbing fibres is a signal for the extinction of conditioned eyelid responses

Javier F. Medina, William L. Nores & Michael D. Mauk

W. M. Keck Center for the Neurobiology of Learning and Memory, and Department of Neurobiology and Anatomy, University of Texas Medical School, Houston, Texas 77030, USA

A fundamental tenet of cerebellar learning theories asserts that climbing fibre afferents from the inferior olive provide a teaching signal that promotes the gradual adaptation of movements^{1–3}. Data from several forms of motor learning provide support for this tenet^{4–8}. In pavlovian eyelid conditioning, for example, where a tone is repeatedly paired with a reinforcing unconditioned stimulus like periorbital stimulation, the unconditioned stimulus promotes acquisition of conditioned eyelid responses by activating climbing fibres^{9–12}. Climbing fibre activity elicited by an unconditioned stimulus is inhibited during the expression of conditioned responses^{9–11}—consistent with the inhibitory projection from the cerebellum to inferior olive^{6,13}. Here, we show that inhibition of climbing fibres serves as a teaching signal for extinction, where learning not to respond is signalled by presenting a tone without the unconditioned stimulus. We used reversible infusion of synaptic receptor antagonists to show that blocking inhibitory input to the climbing fibres prevents extinction of the conditioned response, whereas blocking excitatory input induces extinction. These results, combined with analysis of climbing fibre activity in a computer simulation of the cerebellar-olivary system^{14–16}, suggest that transient inhibition of climbing fibres below their background level is the signal that drives extinction.

To examine how inhibitory inputs to the climbing fibres contribute to extinction of the conditioned response, we infused the GABA (γ -aminobutyric acid) antagonist picrotoxin into the contralateral inferior olive of well trained rabbits undergoing extinction. Twenty rabbits were initially included in the study, of which four were found through histological methods to have cannula placements in the correct region of the inferior olive (two of these four placements are shown in the left column of Fig. 1d). Thus all of our figures and findings report data from these four animals. Rabbits were trained initially for five daily sessions (108 tone plus unconditioned stimulus trials per session) until they had acquired robust eyelid responses. Subsequently, each rabbit received a total of three daily extinction sessions (108 tone alone trials per session) with a different treatment each day (no infusion, continuous artificial cerebrospinal fluid (ACSF) infusion, or continuous infusion with picrotoxin (150 μ M, 0.1 μ l min⁻¹). To maintain high response levels before infusion, each extinction session was preceded by two daily training sessions of the tone plus unconditioned stimulus. With no infusion or infusion with ACSF, the four rabbits showed normal extinction of responses within the 108-trial session (Fig. 1a). In contrast, during intra-olivary infusion of picrotoxin, the same four rabbits maintained robust response levels throughout the entire extinction session (Fig. 1b). A within subjects analysis of variance and subsequent F -test for simple effects revealed that the rates of extinction for no infusion and ACSF infusions were indistinguishable ($F_{11,99} = 0.97$, not significant (NS)), and that both were significantly different from the response rate during picrotoxin infusion ($F_{11,99} = 17.22$ (no infusion) and 16.90 (ACSF), $P < 0.001$) (Fig. 1c).

Unlike experimental manipulations that abolish responses, block learning, or cause extinction, this impairment in extinction of the